Catalysis Today 136 (2008) 258–265

Contents lists available at ScienceDirect

Catalysis Today

journal homepage: www.elsevier.com/locate/cattod

Rhodium supported on thermally enhanced zeolite as catalysts for fuel reformation of jet fuels

Ivan C. Lee *

AMSRD-ARL-SE-DC, US Army Research Laboratory, 2800 Powder Mill Road, Adelphi, MD 20783, USA

ARTICLE INFO

Article history:
Available online 12 May 2008

Keywords:
Jet Fuel
JP8
Fuel reforming
Rhodium
Hydrogen
Fuel processing
Zeolite

ABSTRACT

Autothermal reformation of military jet fuel (1096 ppmw sulfur) was investigated with rhodium supported on thermally stabilized Y zeolite catalysts. The zeolite catalysts were thermally stabilized by ion exchanging with nitrate solutions of rare-earth metals (La, Ce, Sm, Gd, Dy and Er). Surface area analyses indicated that the exchanged zeolite could maintain its porous structure as high as 950 °C instead of 800 °C for a commercial NaY zeolite. The structure of the exchanged zeolite was characterized by X-ray diffraction (XRD). Rh-SmNaY zeolite reforming catalysts were prepared by incipient wetness and organometallic synthesis. The JP8 reforming experiments were performed in a short contact time adiabatic reactor with a monolithic catalyst with the addition of air and steam at a temperature below 920 °C. The effects of steam and fuel-to-air ratio (C/O ratio) were studied. Hydrogen and carbon monoxide were produced as the main products. Durability tests were performed with Rh/SmNaY-zeolite catalysts. This work shows that zeolite based catalysts can convert transportation fuels such as high sulfur jet fuel (over 1000 ppmw S) to syngas for solid oxide fuel cell applications.

Published by Elsevier B.V.

1. Introduction

Fuel cells can provide portable power for battery chargers and auxiliary power without engine idling; however, one of the key challenges is the hydrogen source. Previously, there were literature studies focusing on hydrogen generation by catalytic partial oxidation and autothermal reforming of alkanes, diesel and jet fuel with a standard noble metal supported on high surface area alumina [1–5]. Low C/O ratio, presence of water and the use of Rh instead of Pt can improve the selectivity of syngas (H_2 and CO) formation [1–3]. In one patent catalytic partial oxidation of jet fuel was described [4]. The reaction uses no water and uses oxygen in air as the oxidant. The reaction occurs at temperature greater than 1050 °C. This high temperature limits the choice of construction materials, and the heat management becomes a challenging problem. In another patent, sulfur tolerant catalysts for steam reformation of diesel and jet fuel are described [5] The process uses water as the oxidant, and it needs 3–4 portions of water for each portion of fuel as inputs.

Despite the success of making hydrogen from sulfur containing jet fuel, there is a critical need to develop new catalysts for better coke resistance and for higher sulfur tolerance. Some investigators developed novel perovskite-based, ceria-based and mixed oxide catalysts to reform surrogates of jet fuel and gasoline [6–9]. Varma and co-workers have investigated cerium- and nickel-substituted $LaFeO_3$ perovskite catalysts to reform a JP8 surrogate [6]. JP8 is a kerosene-based jet fuel for the US Army and Air Force. Their results suggested that the nickel-rich catalyst exhibited significant coking, but the addition of cerium greatly enhanced coking resistance of the catalysts. Qi et al. proposed that partially substituting La with Ce at the A-site of $LaNiO_3$ would improve oxygen mobility, thermal stability and catalyst durability [7]. Shekhawat et al. developed Rh-Ce-Zr mixed oxide catalysts for the reformation of *n*-tetradecane with 1-methylnaphthalene or dibenzothiophene [8]. In a recent patent, Krumpelt et al. described sulfur tolerant catalysts for autothermal reformation of gasoline and diesel [9]. At their selected federates of water, air and blended gasoline surrogate, the total syngas (H_2 + CO) concentration (water-free, He-free) was between 73% and 81%.

Zeolite is a common fluid catalytic cracking (FCC) catalyst for hydrocarbons. Y zeolite is the main component with ZSM-5 as an additive. The typical reaction involves hydrocarbon molecules diffusing through the matrix pores into the zeolite crystal. Only certain molecules with certain molecular diameters can penetrate the zeolite structure. A typical temperature range for FCC reaction is from 480 to 550 °C with a contact time of 1–4 s [10]. Zeolite is useful to remove aromatics from diesel fuel by ring-contraction and ring-opening of aromatics such as tetralin [11]. There are

* Tel.: +1 301 394 0292; fax: +1 301 394 0273.
E-mail address: ilee@arl.army.mil.

0920-5861/$ – see front matter. Published by Elsevier B.V.
doi:10.1016/j.cattod.2008.03.027

several reviews on the mechanism of catalytic cracking over solid-acid catalysts [10,12,13]. Protolytic cracking mechanism, bimolecular cracking mechanism and other mechanisms were discussed in detail in these reviews.

It is a common practice of refineries to add rare-earth elements to the zeolite to form ultra-stable Y zeolite (USY). During the regeneration cycles in a FCC unit, additions of rare-earth cations prevent dealumination and improve thermal stability [14]. Several investigators recently studied the role of rare-earth ions for hydrocarbon cracking over Y zeolite [15–17]. A recent study has identified that the role of rare-earth cations in Y zeolite for hydrocarbon cracking is to ensure the retention of high Bronsted acid site density under hydrothermal conditions [15]. These investigators proposed that the zeolite elasticity was increased to lower the composite activation barriers for hydride transfer and β-scission reactions. de la Puente et al. suggested that the hydrogen transfer properties in conversion of cyclohexene increased with the Bronsted acidity and the ionic radius of various rare-earth elements [16]. Liu et al. proposed that the modification of rare-earth directs more hydrocarbons into the pores of Y zeolite to be converted and reduces the possibility of naphtha olefin forming through surface cracking reactions [17].

The main objective of this work is to investigate the usefulness of zeolite as a high surface area support in reforming catalysts. This new class of zeolite reforming catalysts will be evaluated by converting high sulfur transportation fuel (1000 ppmw S or above) to hydrogen with a relative small steam-to-carbon ratio (1 or less). One recent study shows that zeolite catalyst converts methane into hydrogen for fuel cell applications [18] while another study used zeolite as a FCC prereformer to crack the fuel into smaller hydrocarbons [19]. However, zeolite has not been studied as a reforming catalyst for hydrogen generation from transportation fuels. This paper will first discuss the catalyst synthesis and characterization. Then hydrogen generation with millisecond contact time will be demonstrated.

2. Experimental

2.1. Material synthesis

A commercial NaY zeolite (Zeolyst, CBV 100, Si/Al ratio = 5.1) was first exchanged with a 2 M ammonia nitrate solution. The suspension was then centrifuged and washed with de-ionized water 3 times. The exchange-centrifuge-washing process was then repeated twice. The solid (NH_4-NaY zeolite) was dried in a vacuum furnace at 60 °C for 5 h and 120 °C for 1 h. The dried solid was then exchanged with 0.1, 0.2 or 0.4 M nitrate solutions of rare-earth elements (RE = La, Ce, Sm, Gd, Dy or Er) for 68 h. The centrifuge-washing sequence was repeated 3 times. The solid (RE-NaY zeolite) was dried in a vacuum furnace at 60 °C for 5 h and 120 °C for 1 h. Finally, the solid was heated treated in a tube furnace with flowing air at 600 °C.

Four Rh-based catalysts were prepared in this work (Table 1). A standard Rh-alumina foam catalyst (Catalyst 1) was prepared by incipient wetness. The alumina monolith foam (Vesuvius, 80 ppi, 1 in. diameter, 0.5 in. thickness) was wash-coated with 5 wt% γ-alumina to roughen the catalyst surface and to increase its surface area. Then the foam was calcined in a box furnace at 700 °C for 15 h. An aqueous $Rh(NO_3)_3$ solution was added dropwise to the foam, and the resultant foam was calcined in the box furnace at 700 °C for 15 h.

The Rh-SmNaY zeolite foam catalyst (Catalyst 3) was also prepared by incipient wetness similar to the preparation of standard Rh-alumina foam catalyst (Catalyst 1). The monolith foam was coated with 5 wt% SmNaY zeolite without any γ-alumina coating. The incipient wetness procedure would deposit Rh particles on the surface of the zeolite-coated foam. The SmNaY zeolite was obtained from previously described ion-exchanged method with 0.4 M $Sm(NO_3)_3$. A control catalyst (Catalyst 2) was prepared with NaY zeolite without any rare-earth thermal stabilizer.

The ship-in-the-bottle procedure of synthesizing Rh nanoclusters inside the supercages of NaY zeolite was investigated by Weber and Gates [20]. In this study the same organometallic approach was applied to insert the Rh nanoclusters inside the supercages of rare-earth exchanged NaY zeolite. The SmNaY zeolite was first calcined with flowing air at 300 °C for 12 h and then was degassed in a vacuum furnace at 250 °C for 12 h. The zeolite was then transferred into an argon-filled glove box. The zeolite was added to an air-tight flask with a mixture of desirable amount of $Rh(CO)_2(acac)$ in pentane. The slurry was stirred at room temperature for 3 days. The solid was separated by vacuum filtration, and it was transferred to an air-tight quartz tube reactor. The resulting solids were carboxylated in 5% CO (balanced Ar) at 125 °C for 8 h and then decarboxylated in pure He at 200 °C for 12 h. Elemental analyses of Rh-SmNaY powder were performed by Galbraith Laboratories, Knoxville, TN. The loadings of Rh and Sm in Rh-SmNaY powder were determined to be 2.07 and 4.44 wt%, respectively. Next the Rh-SmNaY powder was mixed with an alumina binder to form a slurry, and then the slurry was coated onto a ceramic alumina monolith foam. The finished catalyst foam was labeled as Catalyst 4. The Rh loading of this catalyst foam was 0.0508 wt%.

2.2. Material characterization

The thermal stability of these exchanged zeolite samples was examined by measuring the specific surface area with BET analysis (Micromeritics, ASAP 2000) after sample annealing. Each annealing was performed in a tube furnace with flowing air at an evaluated temperature for 3 h.

X-ray diffraction (XRD) experiments were performed with a Rigaku Ultima III diffractometer using a Cu Kα radiation source working at 40 kV and 44 mA. The XRD patterns of Sm, Dy or Er-loaded zeolite were measured in Bragg-Brentano (BB) configuration to identify any impurities or secondary phase, as well as in parallel beam (PB) configuration to determine the lattice constant or unit cell parameter. The XRD patterns were generated by measuring 2θ from 4° to 80° with a step size of 0.02° and measuring time of 12 s per step (BB) or 24 s per step (PB).

2.3. Fuel characterization

Sulfur analysis of a military jet fuel (JP8) sample was performed with an Agilent gas chromatography (GC) with an Ionics/Sievers

Table 1
Preparation of reformation catalysts in this study

Catalyst no.	Materials	Weight of finished catalyst foam (g)	Coating (wt%)	Rh loading (wt%)
1	Rh/γ-alumina	6.505	3.51 (alumina)	2.50
2	Rh/NaY zeolite/γ-alumina	6.432	2.55 (NaY zeolite)	1.97
3	Rh/Sm-NaY zeolite/γ-alumina	6.518	3.41 (Sm-NaY)	2.13
4	Rh/Sm-NaY zeolite/γ-alumina	6.410	2.40 (Sm-NaY)	0.0508

sulfur chemiluminescence detector (SCD). The details of the sulfur analysis were given elsewhere [21]. A series of standards were prepared for calibration of the GC, and iso-octane was chosen as a solvent. The jet fuel sample was diluted with iso-octane. 5 μL of the diluted sample was injected into the gas chromatograph with a 10-μL microsyringe. Organosulfur compounds were injected into the GC to match the retention time of organosulfur compounds present in the JP8 samples. The total sulfur content of JP8 sample was determined with a total sulfur analyzer (Analytik Jena, Multi EA 3100).

2.4. Reformation experiments

The same batch of jet fuel was used in all the experiments in this study. The fuel supplier provided the boiling point range which was between 159 and 267 °C. The boiling points for 10%, 20%, 50% and 90% recoveries were 178, 186, 207 and 247 °C, respectively. Both the liquid and gas flows were controlled by mass flow controllers. The jet fuel and water were vaporized before mixing with air. The mixed feed was preheated to about 280 °C. The typical gas hourly space velocity (GHSV) is 350,000 h^{-1} or 10 ms at the reaction temperature 900 °C. The catalysts were used as prepared without any activation process (Table 1). The reformate effluent was cooled in a condenser to separate water and liquid hydrocarbons from the gas stream. The effects of steam (H_2O/C ratio) and carbon-to-oxygen ratio were studied by analyzing the reformate composition on-line simultaneously with a Hamilton Sunstrand mass spectrometer (MS) or an Agilent 3000 micro-gas chromatograph. In the gas chromatography, a molecular sieve column (using argon as carrier gas) separates the carbon monoxide, hydrogen and methane; the Plot U column (using helium as carrier gas) separates the carbon dioxide. The analysis of each injection typically takes 3 min. Due to the limitations of the mass spectrometer, carbon species of 3 or more carbon atoms were not quantified. The fuel conversion is defined in Eq. (1),

$$\text{Conversion}\,(\%) = \frac{\text{Total amount of C}\,(CO, CO_2, CH_4, CH_3CH_3, CH_2CH_2)\,\text{in reformate}}{\text{Total amount of C in feed JP8}} \quad (1)$$

Raw or untreated jet fuel typically contains hydrocarbon from C8 to C17. Since C3–C7 compounds were not quantified in this study, these compounds were not included in the conversion calculation. As a result, the actual conversion would be higher than the above estimation.

The carbon atom selectivity of a species is defined in Eq. (2),

$$\text{C Atom Selectivity of Species A} = \frac{\text{C atoms from Species A}}{\text{Total C atoms in the refomate}} \quad (2)$$

The presence of water in the product stream and sometimes in the reactant stream complicates the definition of H selectivity. There are several ways to define H atom selectivity of a species in the reformate gas mixture. In this study, H atom selectivity of Species A is defined in Eqs. (3) and (4),

$$\text{H Atom Selectivity of Species A} = \frac{\text{H atoms from Species A}}{\text{Total H atoms}\,(\text{reformate} - H_2O_{\text{FEED}})}, \text{if A is not } H_2O \quad (3)$$

$$\text{H Atom Selectivity of } H_2O = \frac{\text{H atoms from } H_2O\,(\text{reformate} - \text{feed})}{\text{Total H atoms}\,(\text{reformate} - H_2O_{\text{FEED}})} \quad (4)$$

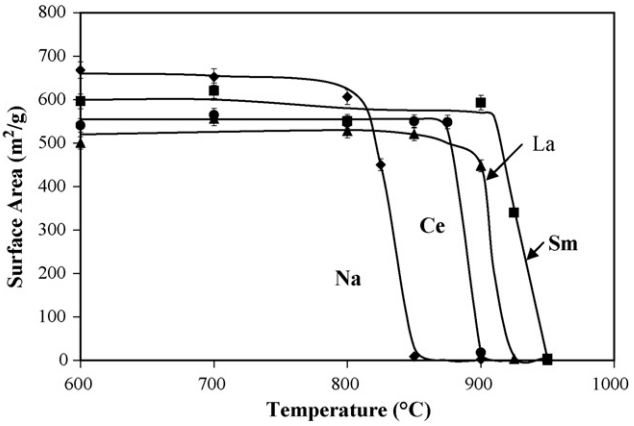

Fig. 1. The thermal stability of selected rare-earth modified NaY zeolites with 0.4 M $RE(NO_3)_3$ precursor solutions.

3. Results and discussion

3.1. Thermal stability of rare-earth loaded zeolites

Fig. 1 illustrates the surface areas of a commercial NaY zeolite and several selected rare-earth thermally stabilized zeolites as a function of annealing temperature. When the commercial NaY zeolite was annealed above 800 °C, its surface area decreased rapidly. This decrease in surface area was due to the breakdown of the zeolite cage structure as confirmed by X-ray diffraction (Fig. 2). The thermal stability of zeolite can be improved by presence of rare-earth elements. Although Ce and La are the most common thermal stabilizers for FCC catalysts, these two rare-earth elements cannot provide sufficient stability at a typical liquid fuel reforming temperature. It is important to note that typical catalytic partial oxidation of JP8 with Rh/γ-Al_2O_3 catalyst is above 1000 °C. However, the reforming temperature can be lowered by addition of steam or by increasing C/O ratio to >1 [3]. To a certain extent, addition of water increases H atom selectivity of H_2, but increasing C/O ratio to >1 decreases H atom selectivity of H_2. Since the goal of this work is to generate H_2 from JP8, the implication of this BET analysis is to run the Rh/rare-earth-stabilized zeolite catalyst with steam addition. The surface areas of the modified NaY zeolites after annealing at 925 °C are summarized in Table 2. Table 2 indicates that Sm, Dy and Er are likely to stabilize the zeolite structure if the reforming temperature can be controlled at or below 925 °C. For

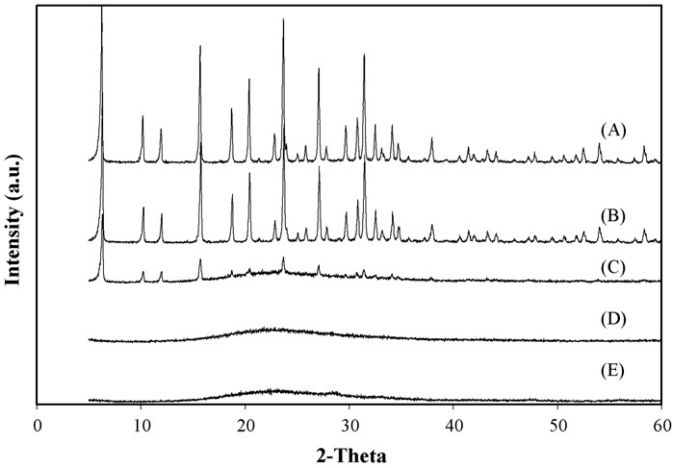

Fig. 2. XRD patterns of NaY zeolites annealed in air background for 3 h at (A) 700 °C, (B) 800 °C, (C) 850 °C, (D) 875 °C and (E) 900 °C.

Table 2
The surface area of modified NaY zeolite by ion exchange with the 0.4, 0.2 or 0.1 M nitrate solution of rare-earth metals

Rare-earth metal	Surface areas after annealing at 925 °C for 3 h (m^2/g)		
	0.4 M	0.2 M	0.1 M
La	<10	NA	NA
Ce	<10	NA	NA
Sm	340	71.7	<10
Gd	<10	NA	NA
Dy	172	253	285
Er	349	484	63.4

NA, not avaliable.

Sm-loaded zeolite, zeolite that exchanged with higher concentration of Sm nitrate solution would give a better thermal stability. In contrast, lower concentrations of Dy or Er nitrate solution are more thermally stable. This difference in stability may be due to the size difference of the +3 cations. The size of +3 cations of Dy or Er is smaller than that of Sm. A detailed analysis of the XRD patterns and elemental compositions of Dy, Er and Sm-loaded zeolite at various loadings are in progress to examine the structure or phase difference at different rare-earth loadings.

3.2. Nature of RE in RE-loaded zeolites (RE = Sm or Er)

The nature of Sm in the Sm-loaded Y zeolite as a function of Sm loading was investigated by XRD. Sm was loaded through ion-exchanged process with 0.1, 0.2 or 0.4 M of $Sm(NO_3)_3$ solution. The XRD patterns of the NaY zeolite and three other Sm-loaded Y zeolites are illustrated in Fig. 3. In consistent with two previous studies [22,23], XRD patterns in Fig. 3 indicated that all the Sm-loaded zeolites maintained a structure similar to the parent NaY zeolite. The XRD patterns also confirmed that there was no secondary phase made of Sm. Previously, Nery et al. have located the rare-earth cations in the zeolite through ion exchange [22]. From their Rietveld refinement of X-ray diffraction pattern, they have proposed that all the rare-earth cations migrated only to the SI′ site which is a 32-fold site located in the sodalite cage. In another recent work, Moreira et al. also investigated the location of cerium in Ce-loaded Y zeolite as prepared from ion-exchanged, precipitation and incipient wetness impregnation [23].

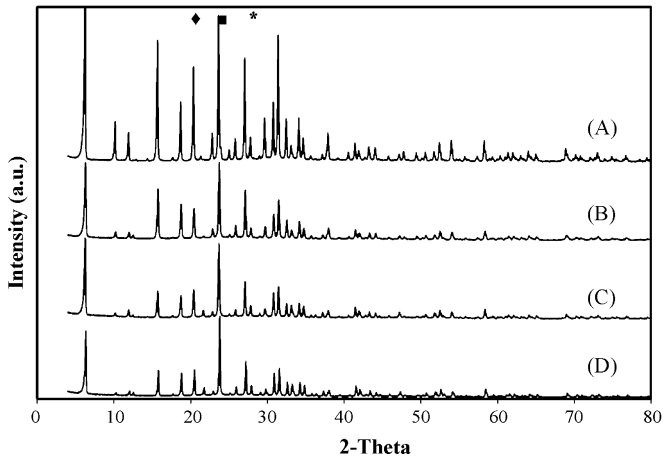

Fig. 3. XRD patterns of (A) NaY zeolite, (B) Sm-loaded zeolite from ion-exchanged with 0.1 M of $Sm(NO_3)_3$, (C) Sm-loaded zeolite from ion-exchanged with 0.2 M of $Sm(NO_3)_3$, and (D) Sm-loaded zeolite from ion-exchanged with 0.4 M of $Sm(NO_3)_3$. (◆) Represents (5 3 3) peak; (■) represents (6 4 2), and (*) represents (5 5 5) peak.

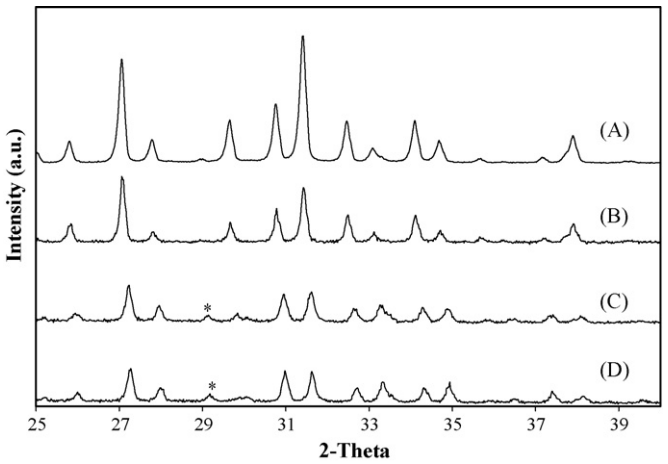

Fig. 4. XRD patterns of (A) NaY zeolite, (B) Er-loaded zeolite from ion-exchanged with 0.1 M of $Er(NO_3)_3$, (C) Er-loaded zeolite from ion-exchanged with 0.2 M of $Er(NO_3)_3$, and (D) Er-loaded zeolite from ion-exchanged with 0.4 M of $Er(NO_3)_3$. (*) Represents (2 2 2) peak of Er_2O_3.

In contrast to well-defined structure of Sm-loaded zeolite, the XRD studies in this work indicated that there was a second phase in Er-loaded zeolite (Fig. 4). As the concentration of $Er(NO_3)_3$ increased from 0.1 to 0.4 M, a new peak emerged at $2\theta = 29.18°$. This peak was assigned to (2 2 2) peak of Er_2O_3. It is known that this (2 2 2) peak is the strongest peak in the XRD pattern of Er_2O_3. At this moment, it is uncertain where the locations of these Er_2O_3 particles are. They may be inside and/or outside the supercages of the NaY zeolite. If the Er_2O_3 particles occupied some fraction of the supercage, some hydrocarbons may become too big to enter the supercage during fuel reformation. If the Er_2O_3 particles were outside the supercage, the interaction between Er_2O_3 and Rh particles may affect the reforming activities other than Er being a thermal stabilizer. Although the 0.2 M Er precursor concentration resulted in the highest surface area zeolite overall (Table 2), the presence of this second phase (Er_2O_3) will limit the validity for a direct comparison of alumina and zeolite supports. Therefore, Sm was selected as the zeolite stabilizer in this work.

In additional to identification of any potential secondary phase, XRD was utilized to determine the unit cell parameter of Sm, Dy or Er-loaded NaY zeolite. The unit cell parameter of zeolite decreased when the concentration of $Sm(NO_3)_3$ solution increased to 0.4 M (Table 3). The unit cell parameters were calculated from the average of (5 3 3), (6 4 2) and (5 5 5) peaks. The decrease in unit cell parameter indicated that the Sm cations replaced the Na cations in the Y zeolite structure. This is consistent with findings in a previous study [22]. Table 3 also shows a similar trend of decreasing unit cell parameter for Dy or Er-loaded zeolite. This trend also indicated that Dy^{3+} and Er^{3+} replaced the Na^+ in the zeolite structure. However, the contraction in unit cell parameter for Er-loaded zeolite is more severe than that for Sm-loaded zeolite due to smaller cationic radius of Er^{3+}.

Table 3
Determination of unit cell parameters of RE-NaY with XRD in parallel beam configuration

Concentration of $RE(NO_3)_3$ solution (M)	Unit cell size, a_o (Å)		
	RE = Sm	RE = Dy	RE = Er
0	24.65	24.65	24.65
0.1	24.65	24.42	24.44
0.2	24.46	24.42	24.38
0.4	24.45	24.38	24.38

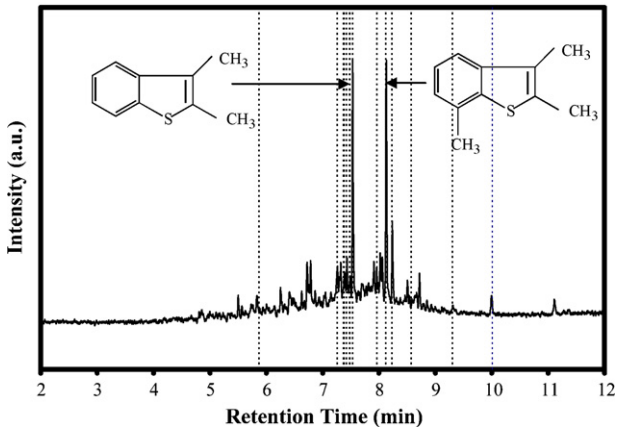

Fig. 5. Sulfur analysis of JP8 fuel sample with GC-SCD. The dotted line represents the retention times of organosulfur standards.

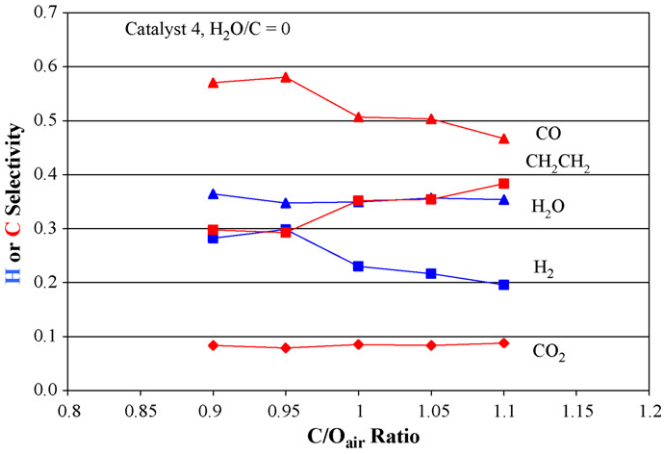

Fig. 6. Product selectivity of jet fuel reformation with Catalyst 4 at $H_2O/C = 0$. The total feed flowrate was kept constant at 6 SLPM, and this total flowrate corresponded to GHSV of 240,000 h^{-1} or catalyst contact time of 15 ms at 900 °C.

3.3. Sulfur analysis of jet fuel

The sulfur content of the military jet fuel sample was determined to be 1096 ppmw. The organosulfur compounds were benzothiophenes with one or more methyl group substitutions, including 2,3-dimethylbenzothiophene and 2,3,7-trimethylbenzothiophene. The sulfur chromatogram and assignments of these two major organosulfur compounds are shown in Fig. 5. A detailed study on the sulfur compositions in JP8 can be found in a recent report [21].

3.4. JP8 reformation

The feed temperature of reactants was 280 °C, and the catalyst bed was initially heated to 300 °C. When the feed reactants contacted the catalyst surface, the reactor lighted off within seconds and the backface catalyst foam temperature increased to the range of 950–980 °C for the catalytic partial oxidation experiments. With steam addition, the catalyst temperature was between 800 and 900 °C. Since Catalyst 2 (Rh/NaY-zeolite) did not have any rare-earth element to stabilize the zeolite cage, the H atom selectivity of H_2 dropped continuously once the reformation started. The zeolite cage collapsed as suggested by Fig. 2, and Catalyst 2 lost its reforming activities within minutes.

For other three catalysts, the oxygen conversion was 100% since no oxygen breakthrough was observed. The JP8 conversions were >90% in all cases. Table 4 summarizes the reformate compositions in a water-free and nitrogen-free basis for Catalysts 1, 3 and 4 under some selected feed conditions. Since the CO can be used either as a fuel for high temperature fuel cells (such as solid oxide fuel cells) or as a reducing agent to reduce water to hydrogen through water-gas shift reaction, it is important to compare the total syngas (H_2 + CO) concentrations. Table 4 shows that each of these three catalysts produces optimum amount of syngas under different feed conditions. The highest syngas concentrations for Catalysts 1, 3 and 4 were 93.0%, 93.2% and 83.6%, respectively (Runs C, D and B). However, it should be noted that comparisons of product selectivity in the subsequent sections are also important. For instance, Catalyst 4 usually gives a high H atom selectivity of H_2O.

When C/O = 0.90 and $H_2O/C = 1.0$, Catalyst 4 produced more syngas than Catalyst 3 (Runs A and B). Although the Rh loading in Catalyst 4 is about 40 times less than that in Catalyst 3, Rh particles inside the supercage of zeolite proves to be an active JP8 reforming catalyst. The syngas production with Catalyst 3 is also very sensitive to H_2O/C ratio. If the H_2O/C ratio was reduced by half (Runs A and F), the hydrogen concentration in the reformate increased to 39.8% from 28.0%. If C/O increased to 0.95 from 0.90 (Runs A and D), the syngas production with Catalyst 3 was promoted significantly to 93.2%. When C/O = 0.90 and $H_2O/C = 0.5$, Catalyst 1 produced more syngas than Catalyst 3 (Runs E and F).

3.4.1. Effect of C/O ratio in catalytic partial oxidation (dry condition)

Fig. 6 shows the product selectivities to synthesis gas (CO, H_2), combustion products (CO_2 and H_2O), and ethylene for the catalytic partial oxidation experiments with Catalyst 4. Methane and propylene were also produced. A previous study [3] has shown that Rh/γ-alumina catalyst heterogeneous syngas production dominates at low C/O ratio while homogeneous olefins production dominates at high C/O ratio. In this work the selectivity to produce syngas is optimum at C/O = 0.95 (Fig. 6). As the C/O increased further, the hydrogen and carbon monoxide selectivities deceased. At the same time the ethylene selectivity increased continuously. However, the selectivity of the combustion products remained almost the same when the C/O ratio increased from 0.9 to 1.1. Although this trend in product selectivity is consistent with a previous study on JP8 reformation with Rh/γ-alumina catalyst [3], the Rh/SmNaY catalyst has a lower H atom selectivity of H_2 than

Table 4
Reformate gas output for reforming JP8 with 1096 ppmw sulfur

Test run	Catalyst	GHSV at 1173 K (h^{-1})	C/O	H_2O/C	H_2 (%)	CO (%)	CO_2 (%)	(H_2 + CO) (%)
A	Catalyst 3	332,000	0.90	1.0	28.0	47.6	7.7	75.6
B	Catalyst 4	332,000	0.90	1.0	34.4	49.2	8.5	83.6
C	Catalyst 1	240,271	0.90	0	42.2	50.9	4.1	93.0
D	Catalyst 3	337,000	0.95	1.0	41.5	52.0	4.6	93.2
E	Catalyst 1	286,000	0.90	0.5	45.4	46.5	6.1	91.9
F	Catalyst 3	286,000	0.90	0.5	39.8	47.6	7.4	87.3

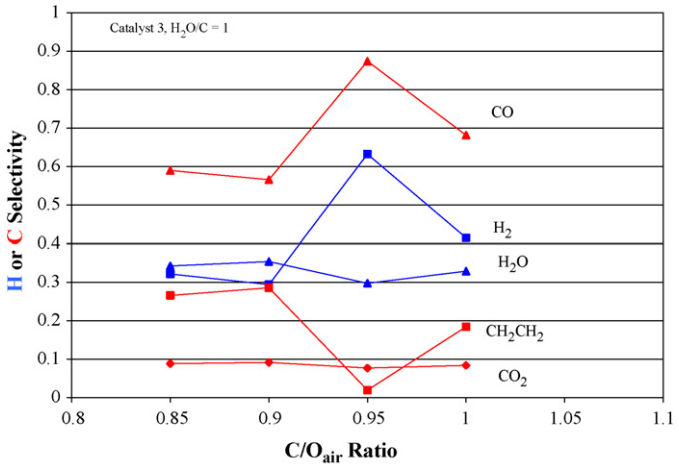

Fig. 7. Product selectivity of jet fuel reformation with Catalyst 3 at $H_2O/C = 1$. The combined feed rate of oxygen and fuel was 6 SLPM, and steam was added at $H_2O/C = 1$. As a result the total flowrate varied from 8.3 to 8.8 SLPM as the C/O ratio increased from 0.9 to 1.1.

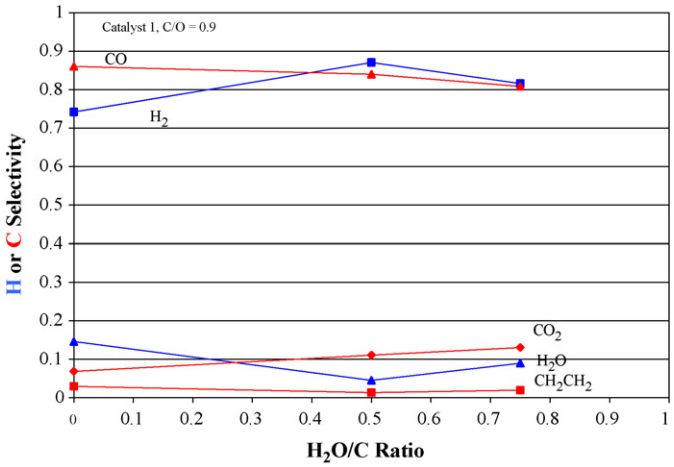

Fig. 9. Product selectivity of jet fuel reformation with Catalyst 1 at C/O = 0.9. The combined feed rate of oxygen and fuel was 6.0 SLPM. As the H_2O/C ratio was increased to 1, the total flowrate was 8.3 SLPM.

the Rh/γ-alumina catalyst. Catalyst 4 selectively produced more water than hydrogen at all C/O ratios. Moreover, this zeolite catalyst also favored olefin formation. Both water production and olefin formation lowers the H atom selectivity of H_2 in Catalyst 4.

In addition, there is an issue of catalyst durability in dry reforming conditions. This set of experiments were started with the C/O ratio at 1.1, and the C/O ratio was gradually decreased to 0.95. There was a gradual increase in catalyst temperature when C/O ratio decreased. When the C/O ratio was further decreased to 0.9, the catalyst performance was stable for 45 min. Then the ethylene production increased rapidly, and the catalyst were destroyed after about 70-min operation at C/O at 0.9.

3.4.2. *Effects of C/O ratio and H_2O/C ratio with steam addition*

Since C/H atomic ratio of heavy hydrocarbons (alkanes and alkenes) is approximately equal to 0.5, $H_2O/C = 1$ is the maximum steam-to-carbon ratio for JP8 reformation without mass penalty of water load in an integrated fuel-cell-fuel-processing system. In other words, the atomic mass balance of this integrated system indicates that the system can recycle up to 1 mole of H_2O for each mole of C in the hydrocarbon feed. For this reason, this work is focusing on steam addition with $H_2O/C \leq 1$.

As shown in Fig. 7, the optimum hydrogen production with Catalyst 3 occurred when the C/O_{air} ratio (or simply C/O ratio) was 0.95. The C atom selectivity of CO followed the same trend as hydrogen while the C atom selectivity of ethylene was a mirror image of the C atom selectivity of CO. The C atom selectivity of CO_2 remained almost the same at all the C/O ratios. In presence of water, the H atom selectivity of H_2 and C atom selectivity of CO with Catalyst 4 decreased as the C/O ratio was increased from 0.9 to 1.1 (Fig. 8). Comparison of Figs. 7 and 8 suggest that the location of Rh clusters, which was controlled by the preparation method, affects the extent of combustion. When the Rh clusters are inside the supercage of zeolite (Catalyst 4), increase in C/O ratio enhances combustion. When the Rh clusters are outside the supercage (Catalyst 3), the product selectivity of combustion products remains the same as the C/O ratio increases.

Catalyst 4 converts JP8 to produce more syngas and less ethylene with steam addition than in dry conditions (Figs. 6 and 8). The addition of water lowered the catalyst back-face temperature by as much as 150 °C. Fig. 8 showed that at C/O = 0.9 the H atom selectivity of H_2 and C atom selectivity of CO were 0.438 and 0.689,

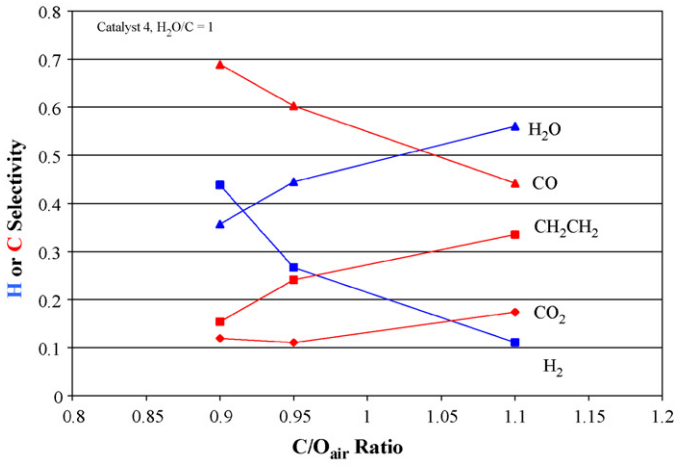

Fig. 8. Product selectivity of jet fuel reformation with Catalyst 4 at $H_2O/C = 1$. The combined feed rate of oxygen and fuel was 6 SLPM, and steam was added at $H_2O/C = 1$. As a result the total flowrate varied from 8.3 to 8.8 SLPM as the C/O ratio increased from 0.9 to 1.1.

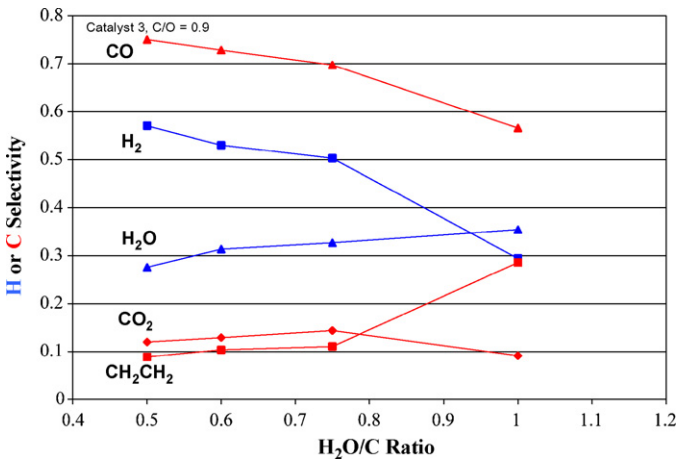

Fig. 10. Product selectivity of jet fuel reformation with Catalyst 3 at C/O = 0.9. The combined feed rate of oxygen and fuel was 6.0 SLPM. As the H_2O/C ratio was increased to 1, the total flowrate was 8.3 SLPM.

respectively. At the same C/O ratio, catalytic partial oxidation with the same catalyst gave H atom selectivity of H_2 of 0.282 and C atom selectivity of CO of 0.571 (Fig. 6). Simultaneously, C atom selectivity of ethylene decreased from 0.298 to 0.154 when the H_2O/C increased from 0 to 1.0. In addition, the presence of water enhanced the formation of combustion products (CO_2 and H_2O) as the C/O ratio increased above 0.95 (Fig. 8). In contrast, Fig. 6 shows no significant change in combustion product selectivity when the C/O ratio increases.

Figs. 9 and 10 illustrate the product selectivity as a function of H_2O/C ratio for Catalysts 1 and 3, respectively. To obtain the maximum H atom selectivity of H_2, the optimum H_2O/C ratio was 0.5 (Fig. 9). The H atom selectivity of H_2 was 0.87 at this optimum H_2O/C ratio, and the remaining H atoms mainly formed H_2O. When H_2O/C increased from 0 to 0.5, H atom selectivity of H_2 increased and C atom selectivity of CO decreased. These changes suggested that the water-gas reaction played an important role with the Rh/γ-alumina catalyst at H_2O/C = 0.5. For Catalyst 3, the optimum H_2O/C ratio for H atom selectivity of H_2 was also 0.5 (Fig. 10). Due to the heat sensitivity of the zeolite catalyst at high temperature, Catalyst 3 was evaluated at H_2O/C ratio greater than 0.5. The H atom selectivity of H_2 dropped dramatically when H_2O/C was greater than 0.75. As H_2O/C ratio increased from 0.5 to 1.0, C atom selectivity of ethylene selectivity increased 3 times. These results implied that the role of the water-gas shift reaction became less important when H_2O/C was greater than 0.5. In case of a zeolite catalyst, excessive water promoted the formation of ethylene and suppressed syngas production.

3.5. Durability of zeolite reforming catalyst

Fig. 11 illustrates the JP8 reforming performance of Catalyst 3 for a continuous 20-h period. The C/O ratio and the H_2O/C ratio were selected so that the catalyst temperature was between 910 and 915 °C during this 20-h period. Most of the changes in product selectivity occurred in the first 10 h, and then stable selectivities were observed for next 10 h. When the reforming activity decayed, heterogeneous syngas production was suppressed and homogeneous olefin production was promoted. During this 20 h of continuous operation, the H atom selectivity of H_2 dropped from 0.50 to 0.40 while C atom selectivity of CO dropped from 0.70 to 0.64. At the same time, C atom selectivity of ethylene went up from 0.11 to 0.17.

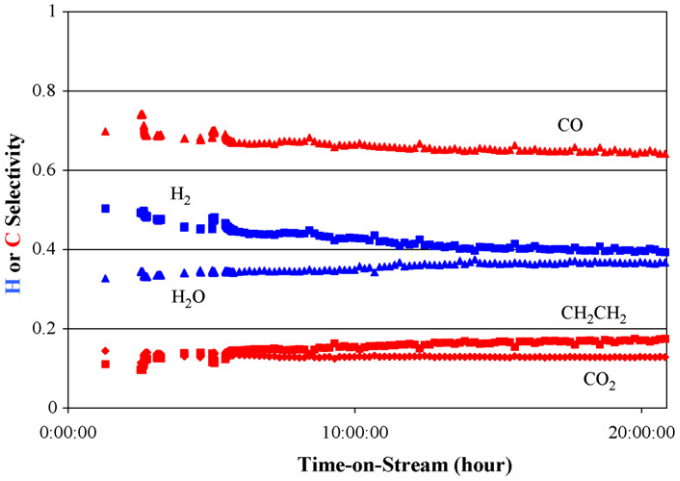

Fig. 11. Catalyst durability of Catalyst 3 during a 20-h continuous JP8 reforming testing. C/O ratio = 0.9, H_2O/C ratio = 0.75 and total feed flow = 7.7 SLPM. The JP8 fuel contained 1096 ppmw sulfur.

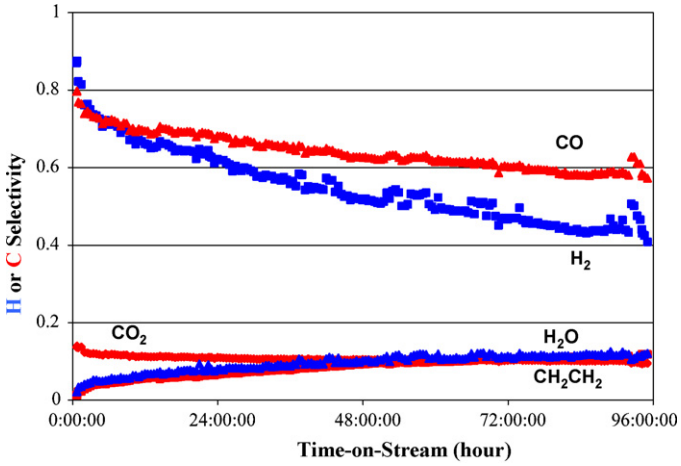

Fig. 12. Catalyst durability of Catalyst 1 during a 96-h continuous JP8 reforming testing. C/O ratio = 0.9, H_2O/C ratio = 0.5 and total feed flow = 7.1 SLPM. The JP8 fuel contained 1096 ppmw sulfur.

Since the C atom selectivity of CO dropped at a lesser extent than H atom selectivity of H_2, the drop in H atom selectivity could only be partially explained by suppression of syngas production. At the same time the rise in H atom selectivity of H_2O could not be due to change in selectivity of combustion since C atom selectivity of CO_2 remained constant. Although H atom selectivity of H_2O increased from 0.33 to 0.37, C atom selectivity of CO_2 remained at 0.13 during this 20-h period. One possible explanation is the enhancement of hydrogen oxidation in which some of the hydrogen from syngas production was oxidized to form water when the catalyst was becoming poisoned during the durability study.

For comparison, Fig. 12 shows the durability of Catalyst 1 with the same batch of JP8 fuel. Although alumina catalyst (Catalyst 1) has a higher initial H atom selectivity of H_2, alumina catalyst degraded much more rapidly than zeolite catalyst (Catalyst 3). The H atom selectivity of H_2 dropped from 0.88 initially to 0.64 after 20 h. Then it further decreased to 0.41 after 96 h.

4. Conclusions

Novel Rh/Sm-Y zeolite catalysts were synthesized by incipient wetness and organometallic method, and these catalysts can convert high sulfur jet fuel (1094 ppmw S) to hydrogen at high reforming temperature (~900 °C). Autothermal reformation of JP8 was investigated with rhodium supported on thermally stabilized zeolite NaY catalysts. The new zeolite catalyst can maintain its reforming activities in a 20-h continuous reformation test with a high sulfur JP8 fuel.

Acknowledgement

The author would like to thank Delphi Automotive for equipment support.

References

[1] J.J. Krummenacher, K.N. West, L.D. Schmidt, J. Catal. 215 (2003) 332.
[2] J.J. Krummenacher, L.D. Schmidt, J. Catal. 222 (2004) 429.
[3] B.J. Dreyer, I.C. Lee, J.J. Krummenacher, L.D. Schmidt, Appl. Catal. A: Gen. 307 (2006) 184.
[4] A. Anumakonda, J. Yamanis, J. Ferrall, US Patent 6,221,280 (April 24, 2001).
[5] T.L. Cable, A.B. Brakas, R.C. Ruhl, C.E. Milliken, US Patent 6,238,816 B1 (May 29, 2001).
[6] P. Erri, P. Dinka, A. Varma, Chem. Eng. Sci. 61 (2006) 5328.

[7] A. Qi, S. Wang, G. Fu, C. Ni, D. Wu, Appl. Catal. A: Gen. 281 (2005) 233.
[8] D. Shekhawat, T.H. Gardner, D.A. Berry, M. Salazar, D.J. Haynes, J.J. Spivey, Appl. Catal. A: Gen. 311 (2006) 8.
[9] M. Krumpelt, J.P. Kopasz, S. Ahmed, R.L. Kao, S.S. Randhava, US Patent 6,967,063 B2 (November 22, 2005).
[10] Y.V. Kissin, Catal. Rev. 43 (2001) 85.
[11] M. Santikunaporn, J.E. Herrera, S. Jogpatiwut, D.E. Resasco, W.E. Alvarez, E.L. Sughrue, J. Catal. 228 (2004) 100.
[12] F. Jentoft, B.C. Gates, Topics Catal. 4 (1997) 1.
[13] A. Corma, A.V. Orchilles, Micropor. Mesopor. Mater. 35–36 (2000) 21.
[14] F.E. Trigueiro, D.F.J. Monteiro, F.M.Z. Zotin, E.F. Sousa-Aguiar, J. Alloys Compounds 344 (2002) 337.
[15] M.A. Sanchez-Castillo, R.J. Madon, J.A. Dumesic, J. Phys. Chem. B 109 (2005) 2164.
[16] G. de la Puente, E.F. Souza-Aguiar, F.M.Z. Zotin, V.L.D. Camorim, U. Sedran, Appl. Catal. A: Gen. 197 (2000) 41.
[17] C. Liu, X. Gao, Z. Zhang, H. Zhang, S. Sun, Y. Deng, Appl. Catal. A: Gen. 264 (2004) 225.
[18] J. Ashok, S.N. Kumar, A. Venugopal, V.D. Kumari, M. Subrahmanyam, J. Power Sources 164 (2007) 809.
[19] T.J. Campbell, A.J. Shaaban, F.H. Holcomb, R. Salavani, M.J. Binder, J. Power Sources 129 (2004) 81.
[20] W.A. Weber, B.C. Gates, J. Phys. Chem. B 101 (1997) 10423.
[21] I.C. Lee, H.C. Ubanyionwu, Fuel 87 (2008) 312.
[22] J.G. Nery, M.V. Giotoo, P. Mascarenhas, D. Cardoso, G.M.Z. Zotin, E.F. Sousa-Aguiar, Micropor. Mesopor. Mater. 41 (2000) 281.
[23] C.R. Moreira, M.M. Pereira, X. Alcobe, N. Homs, J. Llorca, J.L.G. Fierro, P.R. de la Piscina, Micropor. Mesopor. Mater. 100 (2007) 276.